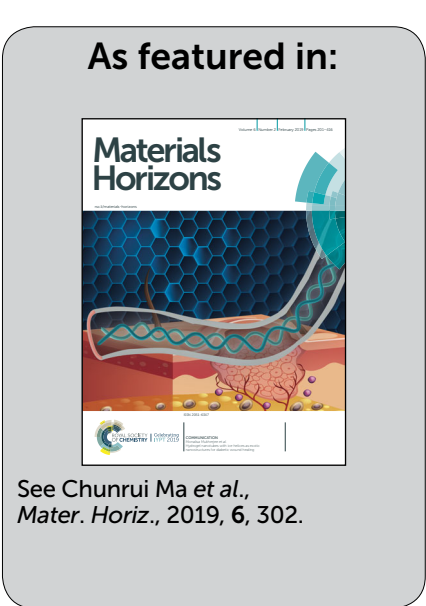


Showcasing the controllable graphene doping state by mechanically bending the ferroelectric gate of a graphene field effect transistor by Associate Prof. Chunrui Ma at the State Key Laboratory for Mechanical Behavior of Materials at Xi'an Jiaotong University (XJTU).

Controlling the Dirac point voltage of graphene by mechanically bending the ferroelectric gate of a graphene field effect transistor

Mechanical strain-controlled graphene doping is simple and reliable; it does not involve the absorption of secondary substances and is recoverable without any change to the graphene. The linear shift of the Dirac point induced by the flexoelectric effect of the ferroelectric gate can not only be used to tune the graphene doping state but also to detect bending curvature.





Materials Horizons



COMMUNICATION

View Article Online



Cite this: Mater. Horiz., 2019, 6 302

Received 23rd November 2018 Accepted 30th November 2018

DOI: 10.1039/c8mh01499i

rsc.li/materials-horizons

Controlling the Dirac point voltage of graphene by mechanically bending the ferroelectric gate of a graphene field effect transistor†

Guangliang Hu, ab Jingying Wu, b Chunrui Ma, b * Zhongshuai Liang, b Weihua Liu, b Ming Liu, b Judy Z. Wuc and Chun-Lin Jiabd

Controlling the Dirac point voltage of graphene is essential for realizing various practical applications of graphene. Here, control of the doping state is achieved in flexible graphene field effect transistors (GFETs) by applying mechanical bending stress. By gradually increasing the bending strain (the decrease of upward/ downward bending radius), the Dirac point (V_{Dirac}) linearly shifts to left/right, which is induced by the flexoelectric effect of the ferroelectric Pb_{0.92}La_{0.08}Zr_{0.52}Ti_{0.48}O₃ (PLZT) gate. In addition, a superior mechanical antifatigue character is obtained in the flexible GFETs, and the doping effect is recoverable. The sensitivity to strain and high bending stability not only offer an easy, controllable and nonintrusive method to obtain a specific doping level in graphene for flexible electric devices, but also highlight the enormous potential of the flexible ferroelectric PLZT-gated GFETs as wearable sensors

1. Introduction

Graphene, a monolayered carbon material with a hexagonal structure, is considered to be a promising material for highperformance nanoelectronics due to its superior chemical stability, high electron mobility, mechanical flexibility and high transmittance. 1-3 In particular, the ambipolar characteristics of graphene-based field effect transistors (GFETs) make them highly competitive with present electronic devices, since graphene can behave as n-type or p-type depending on the type of doping. Until now, great efforts have been made to modulate

Conceptual insights

Graphene has been widely used in various electronic devices. Controlling the doping state or Dirac point voltage (V_{Dirac}) of graphene is essential for its practical applications. Different from traditional methods to modulate the doping state in graphene, such as UV radiation under different gaseous environments and absorption of ionic liquids or gas molecules, here, we propose a new method involving the application of mechanical bending stress on an all-inorganic flexible graphene field effect transistor (GFET). Compared to other methods, the mechanical stress/straincontrolled graphene doping has three advantages: (i) it does not involve the absorption of secondary substances such as gas molecules or ionic liquids; (ii) it is recoverable without any change to the graphene; (iii) the doping operation is simple and reliable. The GFET with a ferroelectric gate (Pb_{0.92}La_{0.08}Zr_{0.52}Ti_{0.48}O₃ thin film) exhibits a linear shift of the Dirac point with increasing the bending stress due to the flexoelectric effect of the ferroelectric gate. These phenomena indicate that it can be used to both tune the graphene doping state through adjusting the curvature and to detect bending curvature through monitoring the variability of $V_{\rm Dirac}$. This makes it enormously useful in flexible electronic devices and deformation sensors.

doping in graphene, such as applying UV radiation in different gaseous environments and absorption of ionic liquid/ionic gel or gas molecules. 4-6 Actually, graphene doping by these methods is realized through surface-transfer doping, which involves electron exchange between graphene and dopants. It is known that a mechanical stress/strain can break centrosymmetry and hence generate a spontaneous electrical polarization (electric charge) in a dielectric material. Therefore, in principle, graphene can be tuned by applying a mechanical stress/strain to the gate (dielectric material) of flexible GFETs. Compared to other methods, mechanical stress/strain tuning method has three advantages: (i) it does not involve the absorption of secondary substances such as gas molecules or ionic liquids; (ii) it is recoverable without any change to the graphene; (iii) the doping operation is simple and reliable. Based on the above advantages, the mechanical stress/strain method is ideal for tuning graphene doping. Unfortunately, research into using mechanical stress/strain for tuning GFETs is currently lacking.

^a State Key Laboratory for Mechanical Behavior of Materials, Xi'an Jiaotong University, Xi'an 710049, China, E-mail: chunrui.ma@mail.xitu.edu.cn

^b School of Electronic and Information Engineering, Xi'an Jiaotong University, Xi'an 710049, China

^c Department of Physics and Astronomy, University of Kansas, Lawrence, Kanas, 66045, USA

^d Ernst Ruska Centre for Microscopy and Spectroscopy with Electrons, Forschungszentrum Jülich, D-52425 Jülich, Germany

[†] Electronic supplementary information (ESI) available. See DOI: 10.1039/

Moreover, because of the rapidly increasing demand for human-machine interfacing, the development of flexible devices has now become one of the greatest technological and societal challenges. 7-12 Flexible thin films are a key component of wearable sensors. Recently, some inorganic functional oxide thin films, such as CuFe₂O₄ and LiFe₅O₈, have been made flexible by directly fabricating the desired thin film on a flexible mica substrate or transferring the desired thin film from a rigid substrate to a flexible substrate through etching a buffer layer between the desired thin film and the rigid substrate. 13,14 It is known that the inorganic ferroelectric thin films as the gate of GFETs can significantly lower the operating voltage, compared with conventional gate materials (SiO₂/Al₂O₃) or organic flexible ferroelectric gate materials. For example, the popular organic ferroelectric gate material poly(vinylidenefluoride-co-trifluoroethylene) (P(VDF-TrFE)) requires an operating voltage of at least ± 5 V, but typically ± 40 V. While these are among the lowest reported for organic ferroelectric gates, the operating voltages of organic gates are significantly greater than those for inorganic ferroelectric gates, such as Pb_{0.92}La_{0.08}-Zr_{0.52}Ti_{0.48}O₃ (PLZT) and PbZr_{0.2}Ti_{0.8}O₃, which have operating voltages of typically less than ± 2 V.^{12,15-17} In addition, GFETs provide a unique platform to design various sensors, since the conductance of the GFET channel is sensitive to interfacial electrical charges with high bipolar electrical susceptibility. 1,18 Using PLZT-gated GFETs, we previously demonstrated the dynamic self-assembly of monolayer molecular ions on graphene, 19 and high sensitivity is anticipated due to the high gate efficiency of the ferroelectric PLZT gate. 6,16 Herein, we designed an all-inorganic flexible ferroelectric-gated GFET based on a PLZT gate on a fluorophlogopite (F-mica) substrate. Remarkably, the GFET Dirac point (V_{Dirac}) could be tuned via linear mechanical bending. Based on the change of the Dirac point, this kind of flexible GFET has broad prospects. Through tuning the curvature, we can obtain the specific Dirac point that we need. This GFET can be used in the fabrication of flexible electronic or optoelectronic devices requiring controllably doped graphene. Furthermore, by monitoring

2. Results

or people.

Communication

Multilayer films of PLZT/La_{0.67}Sr_{0.33}MnO₃/SrTiO₃ (PLZT/LSMO/ STO) were fabricated by Pulse Laser Deposition (PLD) on F-mica. The crystallinity of the films was characterized using X-ray diffraction (XRD) as shown in Fig. S1a (ESI†). Only the (111) peak can be seen for both the STO buffer layer and the LSMO electrode layer on the (001) F-mica substrate. Combined with the φ scans performed on the (002) reflections of LSMO/ STO and the (202) reflections of the F-mica substrate (shown in Fig. S1b, ESI†), LSMO/STO probably forms an epitaxial

the variability of I_D (source-drain current)- V_G (gate voltage) characteristics, the curvature variation can be detected. This

opens up applications in the field of flexible deformation

sensors, for uses such as measuring the motion of soft robots

relationship of $(111)_{LSMO} / (111)_{STO} / (001)_{F-mica}$ and $[1\bar{1}0]_{LSMO} / (111)_{CSMO} / (111)_{CSM$ $[1\bar{1}0]_{STO}/[010]_{F-mica}$. The PLZT film fabricated on LSMO/STO is also highly oriented. Only a minor peak of (101) was detectable besides the main (111) PLZT peak.

A structure of the flexible GFET was designed and its fabrication process is schematically shown in Fig. 1a. The LSMO film layer was used as the back-gate electrode and the Pt layer parts were used as the source-drain electrode. The GFET channel was about 30 µm in length and 50 µm in width. Fig. 1b shows the Raman spectrum of the graphene channel. The intensity of the 2D peak is around twice of that of the G peak, which is anticipated for single-layer graphene. The GFET sample was annealed in a vacuum below 10⁻⁶ Pa for about 24 hours before the electrical transport measurements to remove the residual adsorbates that had attached to the GFET channel during the GFET fabrication process. ¹⁶ The source-drain current (I_D) on a representative PLZT-gated GFET (black) is depicted in Fig. 1c as a function of the gate voltage V_G , with a fixed source-drain bias of V_D = 20 mV. The leakage current through the PLZT gate (blue) was less than 50 nA as shown in the same figure. The Dirac point V_{Dirac} was 0.72 V. The positive V_{Dirac} indicates that the graphene is p-doped, which is attributed to the polarization of the PLZT ferroelectric gate. 16,20

The differential transconductance $g_{\rm m}$ of the PLZT-gated GFET can be obtained from the I_D - V_G characteristics using the formula:

$$g_{\rm m} = dI_{\rm D}/dV_{\rm G}.\tag{1}$$

It is shown in Fig. 1d in the $V_{\rm G}$ range of ± 2 V. The field effect mobility of holes and electrons can be calculated from the peak transconductance using the formula:21,22

$$\mu = g_{\rm m} L / (W C_{\rm G} V_{\rm D}) \tag{2}$$

where, L is the channel length, W is the channel width, V_D is the drain voltage and C_G is the specific capacitance of the gate. The calculated field effect mobility of holes and electrons are $\mu_{h,B}$ = 54.8 cm² V⁻¹ s⁻¹ and $\mu_{e,B} = 58.7$ cm² V⁻¹ s⁻¹, respectively, which are comparable to the results of our previous work using a PLZT-gated GFET on Nb:STO substrate. 18 The reason for the low graphene mobility is complex; defects in the graphene (such as cracks or folding from the transfer procedure), screening effects at the graphene/PLZT interface and nanoscale scattering mechanisms may play important roles. 16,22,23

In order to investigate the tuning effect of mechanical strain on the transfer characteristics of GFET with the PLZT gate, the F-mica substrate was mechanically exfoliated down to few tens of micrometers to obtain good flexibility, and then the GFET device was transferred onto polyimide tape for bending tests. Firstly, the strain was introduced by upward bending. The strain was changed by bending the Polyimide tape at various curvature radii of 12 mm, 10 mm, 8 mm and 6 mm. The I_D - V_G characteristics of the flexible PLZT-gated GFET at different curvature radii are shown in Fig. 2a and the inset is a photo of the bending measurement. Despite little change in I_D at $V_{\rm Dirac}$, which may be caused by the effect of air, the mobilities of holes and electrons were almost the same with increasing the

Materials Horizons Communication

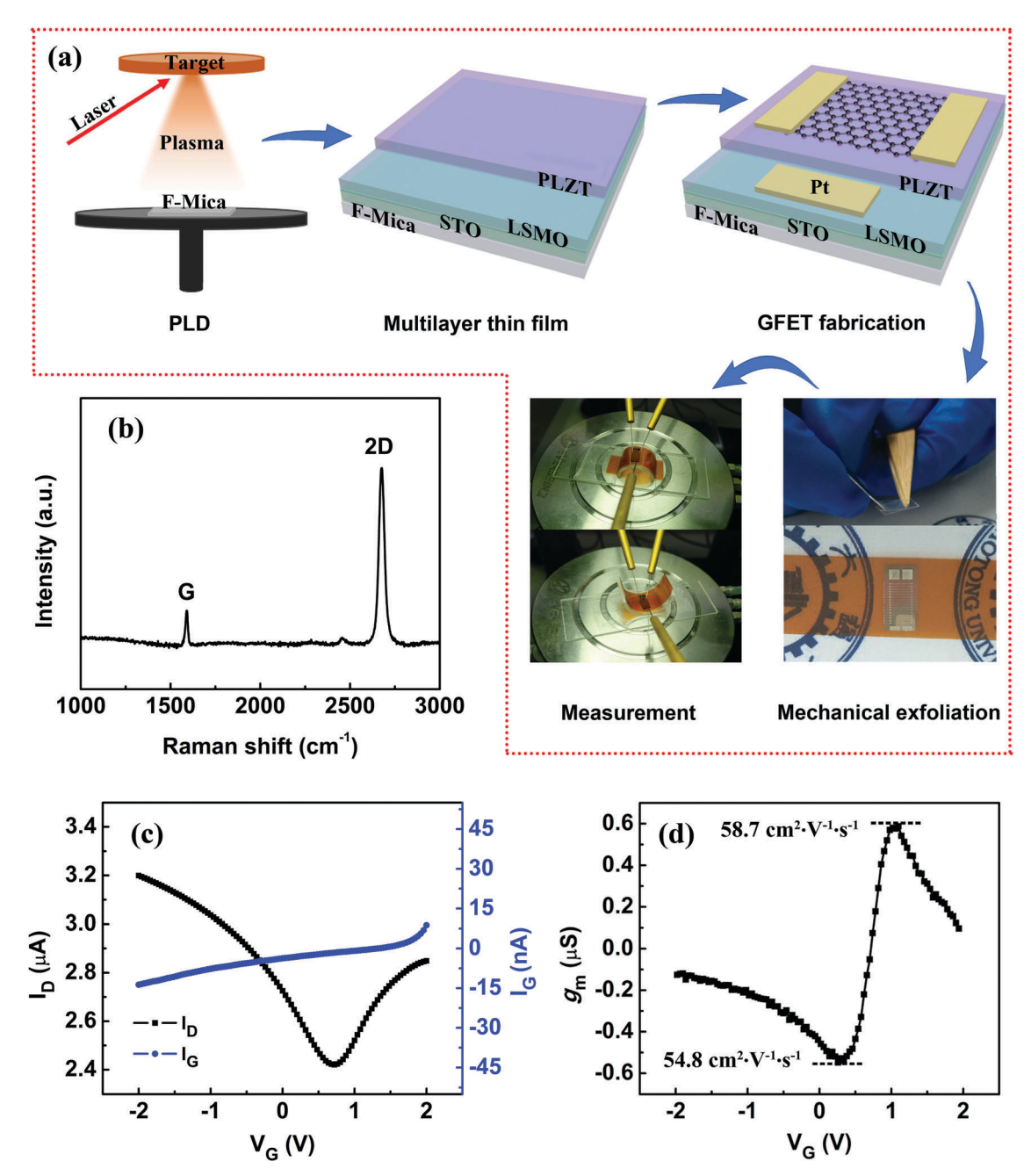


Fig. 1 (a) Fabrication process of the flexible GFET. (b) Raman spectrum of the graphene transferred on the PLZT thin film gate. (c) Transfer characteristics of PLZT ferroelectric gate GFET, measured with a fixed drain bias $V_D = 20 \text{ mV}$. (d) The transfer conduction (g_m) of the PLZT gate GFET corresponding to the $I_D - V_G$ curve in (c).

bending ratio from no bending to a bending radius of 6 mm. $V_{\rm Dirac}$ exhibited a consistent left shift from 0.72 V in a flat state to 0.4 V at the 6 mm bending radius. Interestingly, the $V_{\rm Dirac}$ shift was almost linear with decreasing bending radius, as shown in Fig. 2b (fitted by the red line). Secondly, a strain was introduced by downward bending. As shown in Fig. S2a (ESI†), a similar linear shift of I_D - V_{BG} curves with decreasing bending radius was obtained. However, V_{Dirac} shifted toward a positive value. As shown in Fig. 2c, a linear increase of $V_{\rm Dirac}$ can be seen as the bending radius decreases, with a total right shift of about 0.31 V. In fact, this response is highly reproducible, suggesting that the all-inorganic flexible GFET exhibits excellent flexural fatigue resistance, as shown in Fig. S2b (ESI†). Basically, the I_D - V_G curves of the GFET bending cycle between 1 and 1000 under a bending radius (downward bending) of 6 mm coincide well. The $V_{\rm Dirac}$ values of these curves are extracted and summarized in Fig. 2d. Although $V_{\rm Dirac}$ shows a slight increase of 0.04 V when the bending cycling is above 500, no further changes are observed, suggesting that the PLZTgated flexible GFET has a stable flexural fatigue characteristic.

Communication Materials Horizons

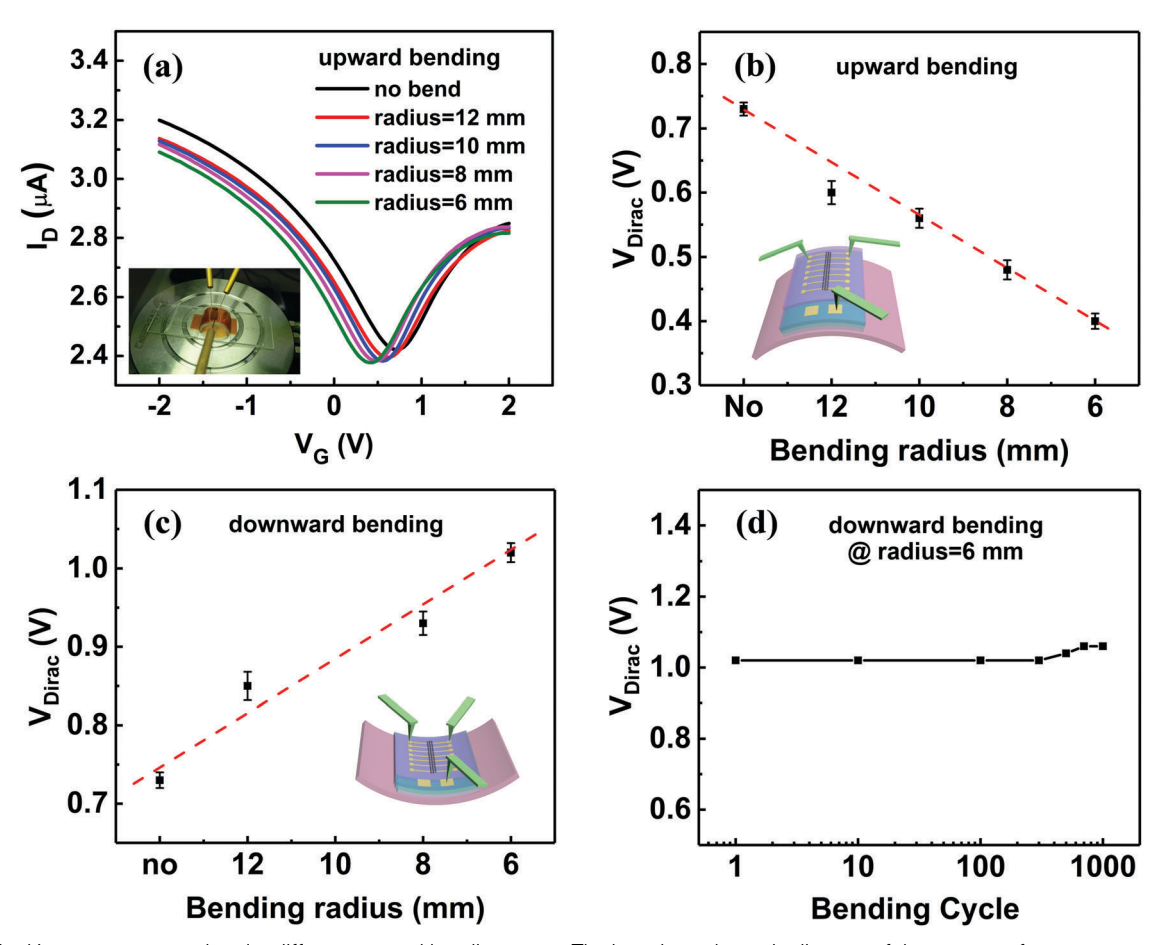


Fig. 2 (a) $I_D - V_G$ curves measured under different upward bending states. The inset is a schematic diagram of the structure for measurement. (b) V_{Dirac} obtained from (a). The inset is the schematic diagram of the structure for measuring the transfer characteristics under upward bending state. (c) V_{Dirac} obtained under different downward bending states. The inset is the schematic diagram of the structure for measurement. (d) The V_{Dirac} as a function of the cycle number obtained from the I_D - V_G characters for the flexible PLZT-gate GFET under a 6 mm downward bending radius.

Similar flexural fatigue resistance for upward bending can be seen in Fig. S3 (ESI†).

The linear shift of V_{Dirac} with the increasing bending curvature (or decreasing bending radius) can be understood based on two factors: one is the GFET channel and the other is the characteristics of the gate, in response to bending. Kundalwal et al.²⁴ stated that the magnitude of the dipole moment per atom of graphene presents a sharp linear decrease (from 0.2 D to 0.03 D) with increasing the radius of curvature from 11.8 Å to 15.2 Å. So, when the radius of curvature is at the millimeter level, as in our case, the magnitude of the dipole moment is too small to be ignored. Therefore, we focused our investigation on curvature-induced polarization of the PLZT ferroelectric gate. The ferroelectric properties of PLZT with LSMO as the bottom electrode and Pt as the top electrode are shown in Fig. 3. Fig. 3a depicts the polarization-voltage (P-V) hysteresis loops at selected maximum applied voltages in the range of 2-20 V. It can be seen that the coercive voltages V_c^+ and V_c^- are asymmetric, especially at high voltage. This is caused by the built-in electric field at the interface between the electrode (Pt/LSMO) and the PLZT thin film. 25 $V_{\rm c}^{+}$ is less than 2 V, meaning that a 2 V gate voltage is adequate to induce sufficient charge density in the GFET channel for electric dipole alignment and a switch in the ferroelectric PLZT gate, as the polarization of PLZTinduced charge in the GFET channel can change the doping state of graphene. Fig. 3b depicts the leakage current density measured as a function of applied voltage, which shows a maximum value of around 1×10^{-7} A cm⁻² at ± 2 V. The low leakage current density observed suggests that the PLZT films have desired high resistivity for gate dielectric applications. Fig. 3c shows the P-V characteristics of PLZT film at the maximum voltage of 2 V under the various upward bending states with curvature radii of 12 mm, 10 mm, 8 mm and 6 mm. An upward shift of the P-V loops can be seen with increasing the upward bending curvature. Fig. 3d and e show the V_c and $P_{\rm r}$ values of these curves, respectively. It can be seen that both V_c^+ and V_c^- decrease linearly with increasing upward bending curvature. The total shifts of V_c^+ and V_c^- are about 0.19 V and 0.16 V, respectively. $P_{\rm r}^+$ and $P_{\rm r}^-$ increase with increasing the upward bending curvature and the total shifts of $P_{\rm r}^{+}$ and $P_{\rm r}^-$ are about 0.21 μC cm $^{-2}$ and 0.22 μC cm $^{-2}$, respectively. However, for downward bending, the P-V loops show an opposite trend, as shown in Fig. 3f. V_c^+ and V_c^- increase (Fig. 3g) and $P_{\rm r}^+$ and $P_{\rm r}^-$ decrease (Fig. 3h) with increasing downward

Materials Horizons Communication

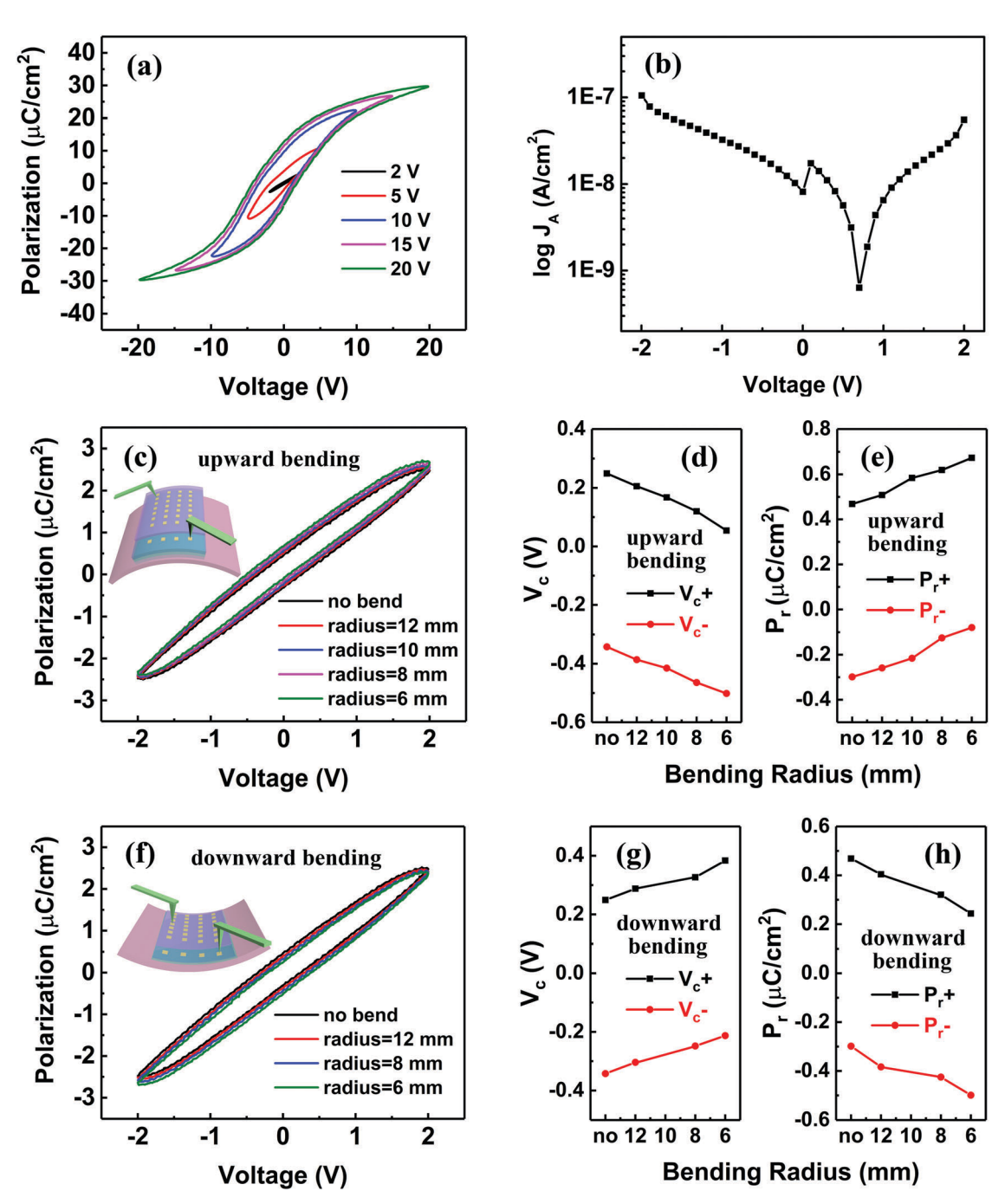


Fig. 3 (a) Typical P-E loops of the PLZT thin film with LSMO bottom electrode and Pt top electrode on F-Mica. (b) Leakage current density of the sample. (c) P-E loops under different upward bending radii at 2 V gate voltage. The inset is a schematic of the measurement. (d and e) V_c and P_r of the loops in (c). (f) P-E loops under different downward bending radii at 2 V gate voltage. The inset is a schematic of the measurement. (g and h) V_c and P_r of the loops in (f).

bending curvature. The total shift of V_c^+ and V_c^- is the same, at around 0.13 V. Meanwhile, the total shifts of P_r^+ and $P_r^$ are about 0.22 μC cm $^{-2}$ and 0.20 μC cm $^{-2}$, respectively. The total polarization of PLZT can be given by the constitutive equation:26

$$P = \chi E + \mu \frac{\partial u}{\partial x}.$$
 (3)

The first term describes the dielectric response with the clamped dielectric susceptibility χ , and the second term describes the flexoelectric response with the flexoelectric coefficient μ . E and $\partial u/\partial x$ are the applied electric field and strain gradient, respectively. As shown in Fig. 4a, the polarization (P_B) induced by the upward bending is up (middle figure), while the polarization induced by the downward bending is down (right figure). From eqn (3) and the strain gradient calculation shown

Communication

(b) (d) ground ground upward bending

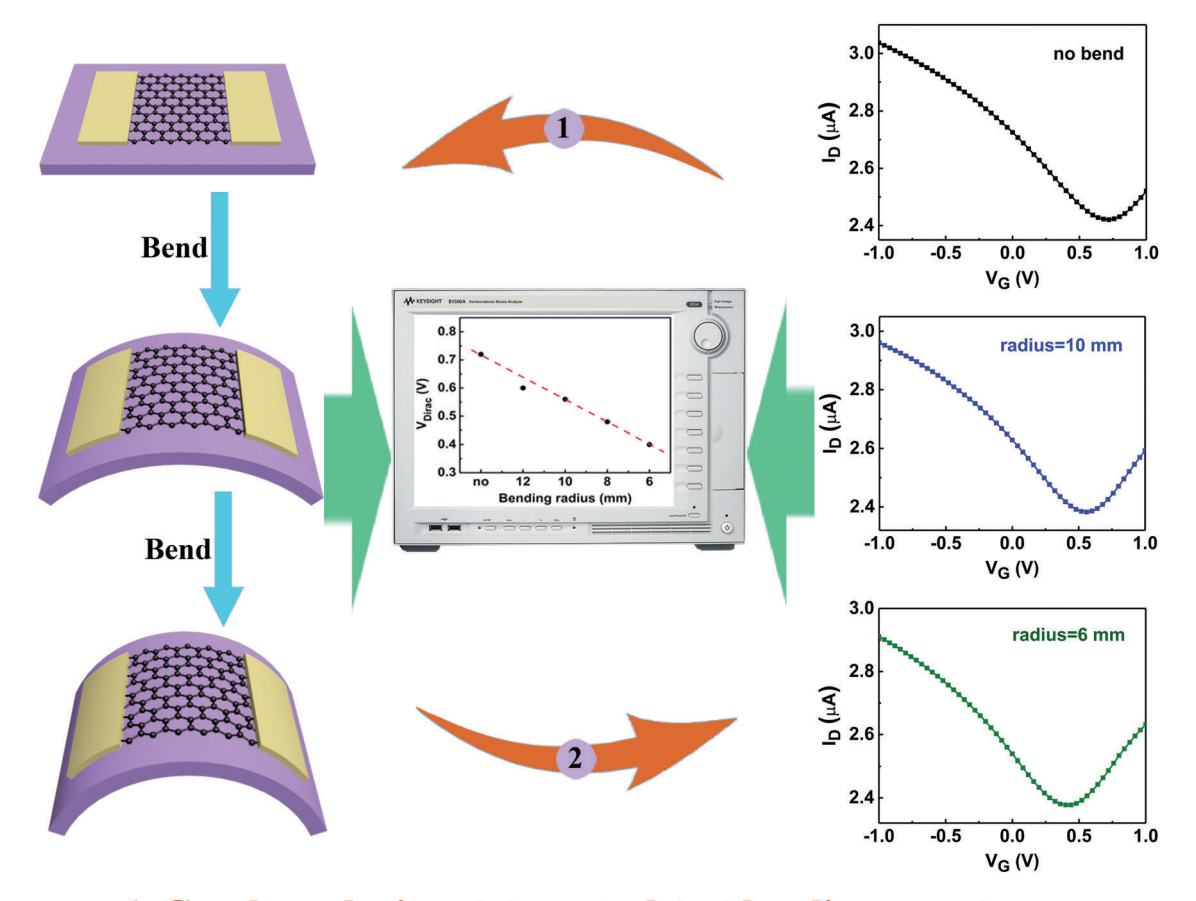
(c) (e) ground ground downward bending

Fig. 4 (a) Schematic diagram of the curvature-induced polarization in PLZT. (b) The polarization in PLZT when positive V^+ and negative V^- are applied on the bottom electrode under upward bending. (c) The polarization in PLZT when positive V^+ and negative V^- are applied on the bottom electrode under upward bending. (d) Negative charge doping in graphene under the upward bending state. (e) Positive charge doping in graphene under the downward bending state.

in Fig. S4 (ESI†), it can be derived that the polarization induced by the strain gradient increases as the bending curvature increases. 26-28 For the case of upward bending (Fig. 4b), when a positive voltage (V^{\dagger}) is applied to the bottom electrode, the direction of polarization induced by the applied electric field $(P_{\rm E})$ is parallel to $P_{\rm B}$. When a negative voltage (V^-) is applied to the bottom electrode, the direction of $P_{\rm E}$ is antiparallel to $P_{\rm B}$. Therefore, the P-V loops will take an upward shift, which is consistent with the measured P-V loops (Fig. 3c). Downward bending (Fig. 4c) generates the opposite behavior, that is, the polarization induced by V^{\dagger} is antiparallel to $P_{\rm B}$, and the polarization induced by V^- is parallel to P_B , making the P-V loops shift downward (Fig. 3f). The upward polarization generated by the upward bending contributes positive charges at the surface of the PLZT thin film. To compensate for the positive charges, negative charges accumulate in the graphene, as depicted in Fig. 4d, leading to a negative-charge-doping effect and a left shifting of V_{Dirac} . With increasing the bending curvature, more positive charges are generated, hence inducing further left shifting of V_{Dirac} . Conversely, the polarization induced by downward bending results in a positive-charge-doping effect in graphene, as shown in Fig. 4e, and a right shifting of V_{Dirac} .

In order to quantitatively analyze the effect of mechanical bending on the doping of graphene, we calculated the charge carrier change (ΔQ) in graphene under bending. As we know, the charge carrier change is related to the Dirac point shift $(\Delta V_{\rm Dirac})$ by $\Delta Q = C_{\rm g} \cdot \Delta V_{\rm Dirac}$, where $C_{\rm g}$ is the back-gate capacitance. From Fig. 2, it can be seen that the total changes of V_{Dirac} under upward bending and downward bending are about 0.32 V and 0.31 V, respectively, when the device is bent from a bending radius of ∞ to a bending radius of 6 mm. As shown in Fig. S5 (ESI \dagger), the capacitance of the back-gate is 0.6 μ F cm⁻², which leads to charge carrier change values of around $0.192 \mu C cm^{-2}$ and $0.186 \mu C cm^{-2}$ in graphene for upward bending and downward bending, respectively. These values are comparable to the polarization change of ΔP_r , as shown in Fig. 3e and h. Based on the experimental results and above discussions, the changes in the polarization of PLZT and $V_{\rm Dirac}$ of GFET are mainly caused by the flexoelectric effect of the PLZT thin film. Moreover, the good flexural fatigue resistance of the PLZT thin film, as shown in Fig. S6 (ESI†), provides the flexible GFET device with stability. These phenomena suggest that mechanical bending can be used to tune the graphene doping state according to the change of the I_D - V_G characteristics (V_{Dirac}), providing great opportunities for wearable mechanical/electronic sensors and flexible electronic devices, as shown in Fig. 5. By monitoring the change of the I_D - V_G characteristics (Dirac point voltage), the curvature variation can be detected (process 1 in Fig. 5), which can be used in the field of flexible deformation sensors to detect mechanical movement, such as human or robotic bending. On the other hand, we can obtain the specific graphene doping state (Dirac point voltage) that we need

Materials Horizons Communication



1. Graphene doping state \longrightarrow detect bending curvature

2. Bending curvature \longrightarrow obtain graphene doping state

Fig. 5 Schematic illustration of the flexible mechanical/electronic sensing system of the inorganic PLZT-gated GFET.

through tuning the mechanical bending stress (curvature), which is very useful for the fabrication of flexible GFETs and other flexible electronic devices (process 2 in Fig. 5).

3. Conclusions

In summary, a tunable Dirac point voltage has been achieved in an all-inorganic flexible GFET through the application of mechanical bending stress. The I_D - V_G characteristics exhibit a continuous change in the Dirac point voltage under mechanical strain (both upward and downward bending). It is exciting that the change of the Dirac point voltage with the mechanical bending strain is linear, resulting from the fact that the flexoelectric effect of the ferroelectric PLZT gate generates additional positive (negative) charges at the surface of the PLZT thin film with upward (downward) mechanical bending and induces electron-doping (hole-doping) effects into graphene. This provides great opportunities for wearable mechanical sensors and flexible electric devices that require a specific doping level in graphene. More importantly, the PLZT-gated GFET devices exhibit excellent stability against flexural fatigue with negligible degradation after 1000 bending cycles. Therefore, the flexible

all-inorganic GFET device is promising for wide applications in flexible sensing systems.

4. Experimental methods

Fabrication of thin film

A buffer layer of ~ 30 nm SrTiO₃ (STO) was first epitaxially grown on the F-mica substrate by a KrF excimer pulsed laser deposition system with a wavelength 248 nm at 800 °C and 50 mTorr oxygen pressure. On the buffer layer, the electrode LSMO (about 45 nm) was epitaxially grown at 700 °C in oxygen atmosphere with a pressure of 50 mTorr. Then, the LSMO/STO double layers were annealed at 700 °C for 15 min under a 400 Torr oxygen atmosphere and cooled down to room temperature at a rate of 5 °C min⁻¹. Afterwards, a PLZT thin film was deposited on the LSMO/STO films with a thickness of 500 nm. The PLZT growth condition was selected under an oxygen pressure of 150 mTorr at 650 °C. After the growth, the PLZT thin films were annealed at the growth temperature for 15 min in pure oxygen (350 Torr) and then naturally cooled down to room temperature. The laser energy density was about 2.0 J cm⁻² with a laser repetition rate of 5 Hz for the LSMO and PLZT films and 3 Hz for STO film, respectively.

Communication **Materials Horizons**

Graphene transfer

A layer of poly-methyl methacrylate (PMMA) was spin-coated on a commercial graphene/Cu sheet with typical dimensions of 1×1 cm² (Muke Nano, Nanjing) and baked in air at 60 °C for 10 min. Before removing the Cu sheet by immersing the graphene sample into a copper etchant (solution of ammonium persulfate stabilization), it was cut into a small sheet of $0.2 \times$ 0.6 cm² in dimension to expose the edge of the copper for etching. The PMMA/graphene was rinsed with deionized (DI) water multiple times after the copper was fully dissolved. The graphene sample was then transferred onto the PLZT with a pre-fabricated Pt source and drain electrodes and baked in air at 150 °C for one hour to eliminate moisture. The PMMA on graphene was removed using acetone, and then the sample was rinsed with isopropyl alcohol to remove residues on the graphene surface.

Characterization

The crystallinity of the PLZT, STO and LSMO thin films was characterized using a high-resolution X-ray diffraction system (HRXRD, PANalytical X'Pert MRD). For the measurement of properties, Pt quadrates of 200 µm in length and 70 nm in thickness were deposited on the PLZT samples by sputtering through a shadow mask. The P-E loops were measured using a TF Analyzer 2000E with FE-Module at a frequency of 1 kHz. The structure of graphene was characterized using a laser Raman spectrometer (LabRAM HR Evolution, HORIBA Scientific), equipped with a standard 633 and 532 nm laser. For the electrical transport property measurements in air, a layer of PMMA was casted onto the graphene channel for passivation. In addition, vacuum cleaning ($<2 \times$ 10^{-6} Torr) was applied to the GFET samples for further removal of the residues in the graphene channel. 16,29 The transport properties of the flexible ferroelectric-gated GFETs were characterized using an Agilent B4155C semiconductor analyzer. Half-cylinders of different diameters were used for the bending measurements.

Conflicts of interest

There are no conflicts to declare.

Acknowledgements

G. H., J. W., Z. L., C. M., M. L. and C.-L. J. acknowledge the support from the National Science Foundation of China (No. 51702255 and 61631166004) and National "973" projects of China (No. 2015CB654903). M. L. and C. M. acknowledge the support from the Fundamental Research Funds for the Central Universities and China Postdoctoral Science Foundation (No. 2015M582649). W. L. acknowledges the support from the National Science Foundation of China (No. 61671368). J. Z. W. acknowledges support in part from US ARO contract W911NF-16-1-0029, and US NSF contracts NSF-DMR-1337737 and NSF-DMR1508494.

Notes and references

- 1 N. O. Weiss, H. Zhou, L. Liao, Y. Liu, S. Jiang, Y. Huang and X. Duan, Adv. Mater., 2012, 24, 5782-5825.
- 2 A. K. Geim, Science, 2009, 324, 1530-1534.
- 3 C. Lee, X. D. Wei, J. W. Kysar and J. Hone, Science, 2008, 321,
- 4 A. Inaba, K. Yoo, Y. Takei, K. Matsumoto and I. Shimoyama, Sens. Actuators, B, 2014, 195, 15-21.
- 5 L. P. Wu, L. Qin, Y. Zhang, M. Alamri, M. G. Gong, W. Zhang, D. Zhang, W. L. Chan and J. Z. Wu, ACS Appl. Mater. Interfaces, 2018, 10, 12824-12830.
- 6 C. Ma, R. Lu, G. Hu, J. Han, M. Liu, J. Li and J. Wu, ACS Appl. Mater. Interfaces, 2017, 9, 4244-4252.
- 7 H. Yu, C. C. Chung, N. Shewmon, S. Ho, J. H. Carpenter, R. Larrabee, T. L. Sun, J. L. Jones, H. Ade, B. T. O'Connor and F. So, Adv. Funct. Mater., 2017, 27, 1700461.
- 8 G. Schwartz, B. C. K. Tee, J. G. Mei, A. L. Appleton, D. H. Kim, H. L. Wang and Z. N. Bao, Nat. Commun., 2013, 4, 1859.
- 9 T. Q. Trung, N. T. Tien, D. Kim, M. Jang, O. J. Yoon and N. E. Lee, Adv. Funct. Mater., 2014, 24, 117-124.
- 10 M. Song, J. Seo, H. Kim and Y. Kim, Sci. Rep., 2017, 7, 2630.
- 11 X. H. Wu, Y. Ma, G. Q. Zhang, Y. L. Chu, J. Du, Y. Zhang, Z. Li, Y. R. Duan, Z. Y. Fan and J. Huang, Adv. Funct. Mater., 2015, 25, 2138-2146.
- 12 X. D. Wang, M. H. Tang, Y. Chen, G. J. Wu, H. Huang, X. L. Zhao, B. B. Tian, J. L. Wang, S. Sun, H. Shen, T. Lin, J. L. Sun, X. J. Meng and J. H. Chu, Opt. Quantum Electron., 2016, 48, 345.
- 13 W. L. Liu, M. Liu, R. Ma, R. Y. Zhang, W. Q. Zhang, D. P. Yu, Q. Wang, J. N. Wang and H. Wang, Adv. Funct. Mater., 2018, 28, 1705928.
- 14 L. K. Shen, L. Wu, Q. Sheng, C. R. Ma, Y. Zhang, L. Lu, J. Ma, J. Ma, J. H. Bian, Y. D. Yang, A. P. Chen, X. L. Lu, M. Liu, H. Wang and C. L. Jia, Adv. Mater., 2017, 29, 1702411.
- 15 N. H. Van, J. H. Lee, D. Whang and D. Kang, Nano-Micro Lett., 2015, 7, 35-41.
- 16 C. Ma, Y. Gong, R. Lu, E. Brown, B. Ma, J. Li and J. Wu, Nanoscale, 2015, 7, 18489-18497.
- 17 C. Baeumer, S. P. Rogers, R. J. Xu, L. W. Martin and M. Shim, Nano Lett., 2013, 13, 1693-1698.
- 18 G. L. Hu, G. P. Pandey, Q. F. Liu, R. S. Anaredy, C. R. Ma, M. Liu, J. Li, S. K. Shaw and J. Wu, ACS Appl. Mater. Interfaces, 2017, 9, 35437-35443.
- 19 G. Hu, C. Ma, W. Wei, Z. Sun, L. Lu, S.-B. Mi, M. Liu, B. Ma, J. Wu and C.-l. Jia, Appl. Phys. Lett., 2016, 109, 193904.
- 20 A. Di Bartolomeo, F. Giubileo, F. Romeo, P. Sabatino, G. Carapella, L. Iemmo, T. Schroeder and G. Lupina, Nanotechnology, 2015, 26, 475202.
- 21 S. C. Sun and J. D. Plummer, IEEE J. Solid-State Circuits, 1980, 15, 562-573.
- 22 G. Fisichella, S. Lo Verso, S. Di Marco, V. Vinciguerra, E. Schiliro, S. Di Franco, R. Lo Nigro, F. Roccaforte, A. Zurutuza, A. Centeno, S. Ravesi and F. Giannazzo, Beilstein J. Nanotechnol., 2017, 8, 467-474.
- 23 F. Giannazzo, S. Sonde, R. Lo Nigro, E. Rimini and V. Raineri, Nano Lett., 2011, 11, 4612-4618.

- **Materials Horizons** Communication
- 24 S. I. Kundalwal, S. A. Meguid and G. J. Weng, Carbon, 2017, **117**, 462–472.
- 25 K. Abe, N. Yanase, T. Yasumoto and T. Kawakubo, J. Appl. Phys., 2002, 91, 323-330.
- 26 P. Zubko, G. Catalan and A. K. Tagantsev, Annu. Rev. Mater. Res., 2013, 43, 387-421.
- 27 F. Ahmadpoor and P. Sharma, Nanoscale, 2015, 7, 16555-16570.
- 28 Q. Deng, M. Kammoun, A. Erturk and P. Sharma, Int. J. Solids Struct., 2014, 51, 3218-3225.
- 29 R. T. Lu, J. W. Liu, H. F. Luo, V. Chikan and J. Z. Wu, Sci. Rep., 2016, 6, 19161.